Validity of the local approximation in iron pnictides and chalcogenides

Patrick Sémon, Kristjan Haule, and Gabriel Kotliar

Phys. Rev. B **95**, 195115 — Published 8 May 2017

DOI: 10.1103/PhysRevB.95.195115

Validity of the Local Approximation in Iron- Pnictides and Chalcogenides

Patrick Sémon[1,2], Kristjan Haule[2], and Gabriel Kotliar[2,3]
[1] *Computational Science Initiative, Brookhaven National Laboratory, Upton, NY 11973-5000, USA*
[2] *Department of Physics and Astronomy, Rutgers University, Piscataway, NJ 08854, USA and*
[3] *Condensed Matter Physics and Materials Science Department, Brookhaven National Laboratory, Upton, NY 11973-5000, USA*

We introduce a methodology to treat different degrees of freedom at different levels of approximation. We use cluster DMFT (Dynamical Mean Field Theory) for the t_{2g} electrons and single site DMFT for the e_g electrons to study the normal state of the iron pnictides and chalcogenides. In the regime of moderate mass renormalizations, the self-energy is very local, justifying the success of single site DMFT for these materials and for other Hunds metals. We solve the corresponding impurity model with CTQMC (Continuous Time Quantum Monte-Carlo) and find that the minus sign problem is not severe in regimes of moderate mass renormalization.

The unexpected discovery of superconductivity in the iron pnictide based materials has opened a new era of research in the field of condensed matter physics.[1] Multiple approaches, starting from weak coupling such as the random phase approximation (RPA) and strong coupling approaches using lessons learned from the t-J model, have been proposed, but there is not yet consensus in the community of what constitutes the proper theoretical framework for describing these systems.[2] It has been proposed that iron pnictides and chalcogenides are important not only because of their high temperature superconductivity, but because their normal state properties represent a new class of strongly correlated systems, the Hunds metals. They are distinct from doped Mott Hubbard systems in that correlation effects in their physical properties derive from the Hunds rule coupling J, rather than the Hubbard U.[3,4] Many other interesting Hunds metals have been recognized, as for example Ruthenates[5] and numerous 3d and 4d compounds[6].

Dynamical Mean Field Theory[7](DMFT) and its cluster extensions[8,9] have provided a good starting point for the description of Mott Hubbard physics. It is now established that it describes many puzzling properties of three dimensional materials such as Vanadium oxides near their finite temperature Mott transition.[10] In materials such as cuprates, as the temperature is lowered, the description in terms of single site DMFT gradually breaks down. New phenomena such as momentum space differentiation and the opening of a pseudogap takes place,[11–35] and cluster DMFT is essential. How different cluster sizes and methods capture these effects has been explored intensively.[14,29,36–41] The iron pnictides and chalcogenides have been extensively studied using LDA+DMFT by several groups.[3,4,42–44] It has been argued using the GW method, that the frequency dependence of low order diagrams in perturbation theory in these materials is very local.[45] However, because of the difficulties posed by the multiorbital nature of these compounds, the accuracy of the local approximation beyond the GW level has not been examined and is the main goal of this paper.

Building on the work of Ref. 46, we introduce a cluster extension for the treatment of iron pnictides, which is numerically tractable using CTQMC. By comparing single site and cluster DMFT, we establish that in a broad range of parameters where the mass renormalizations are of the order of 2 to 3, which corresponds to the experimental situation in many iron pnictides and chalcogenides, the local approximation is extraordinarily accurate, justifying the success of a very large body of work.

For simplicity, we use in this work a tight-binding hamiltonian $\mathbf{h}_0(\mathbf{k})$ of $FeAs$ layers with As treated in second order perturbation theory, as presented by M. J. Calderón et al.[47] For the hopping amplitudes the values suggested for $LaOFeAs$ are taken and scaled such that the bandwidth is $\approx 4eV$.[48] However, the main conclusions of this work should not be very sensitive to the parameterization used. The wave vectors $\mathbf{k}$ label the irreducible representations of a glide-mirror symmetry group instead of the usual translation symmetry group, so that the Brillouin zone contains 1 Fe atom instead of 2 Fe atoms, with hole pockets at the M and Γ points and electron pockets at the X and Y points. Notice here that this unfolding, which is exact in two dimensions, is not exact when the $FeAs$ layers are coupled, i.e., a translation operation perpendicular to the layers does not commute with a glide mirror operation along the layers, and the corresponding symmetry group is not abelian. The correlations of the electrons within a d-shell are captured by adding a local Coulomb interaction, parametrized by the Hubbard repulsion U and the Hund's rule coupling J, see Appendix for more details.

We solve this model using DMFT and Dynamical Cluster Approximation (DCA). DMFT starts by approximating the lattice self-energy locally with that of a single site impurity model. This neglects all $\mathbf{k}$-dependence of the lattice self-energy. DCA retains some of the momentum dependence by first cutting the Brillouin zone into patches of equal size, each patch $\mathcal{P}_{\mathbf{K}}$ enclosing a coarse grained momentum $\mathbf{K}$. The lattice self-energy is then approximated by a piecewise constant function over the patches and identified with that of a cluster impurity model written $\mathbf{K}$-space. In this work, we choose a minimal patching[46] which takes into account both the symmetries and the electron-hole pocket structure of the

Brillouin zone, see Fig. 1. One patch ($\mathcal{P}_+$) encloses the

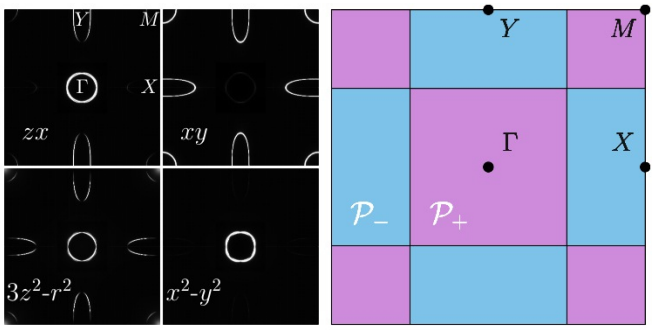

FIG. 1. Left panel: Orbital character of the Fermi surface in the unfolded Brillouin zone of the tight-binding hamiltonian[47] used in this work. Right panel: Tiling of the Brillouin zone in two patches $\mathcal{P}_+$ and $\mathcal{P}_-$, enclosing the holes pockets at Γ and M and the electron pockets at X and Y respectively. This patching is compatible with the lattice symmetries.

holes at $(0,0)$ and (π,π) and the other patch ($\mathcal{P}_-$) encloses the electrons at $(\pi,0)$ and $(0,\pi)$.

The (cluster) impurity model is solved by continuous-time Monte-Carlo sampling of its partition function, written as a power series in the hybridization between impurity and bath (CT-HYB)[49–51]. This solver is well suited for strong and/or complex interactions as arising in the context of realistic material simulations. The price to pay is a complexity that scales with the dimension of the Hilbert space of the impurity.

The 5 d-orbitals split into $e_g = \{3z^2 - r^2, x^2 - y^2\}$ and $t_{2g} = \{yz, zx, xy\}$ degrees of freedom. Since the latter contribute the dominant character of the bands near the Fermi level, an idea to obtain a cluster impurity problem amenable for CT-HYB is to apply DCA only to the t_{2g} orbitals, while the e_g orbitals are treated within DMFT. To make this idea more specific, it is convenient to consider DMFT and DCA as approximations of the Luttinger-Ward functional[52] $\Phi_{UJ}[\mathbf{G}]$, a functional of the dressed Green function $\mathbf{G}$ which depends on the interacting part of the problem only, that is U and J in our case. Its derivative is the self-energy, and together with the Dyson equation

$$\mathbf{G}_0^{-1} - \mathbf{G}^{-1} = \mathbf{\Sigma}[\mathbf{G}] = \frac{1}{kT}\frac{\delta\Phi_{UJ}[\mathbf{G}]}{\delta\mathbf{G}}, \qquad (1)$$

the (approximate) Luttinger-Ward functional determines hence the (approximate) solution of the problem with bare Green function $\mathbf{G}_0$. Diagrammatically, the Luttinger-Ward functional is the sum of all vacuum-to-vacuum skeleton diagrams, and DMFT keeps only the diagrams with support on a site. In momentum space, this corresponds to neglect conservation of momentum at the vertices, which is partially restored in DCA by conserving at least the coarse grained momentum $\mathbf{K}$. We call the corresponding functionals $\Phi^{\text{loc}}_{UJ}[\mathbf{G}]$ and $\Phi^{\text{cl}}_{UJ}[\mathbf{G}]$, respectively. In this functional formulation, the mixed DMFT-DCA treatment of the orbitals that we propose consists in approximating the lattice functional as

$$\Phi_{UJ}[\mathbf{G}] = \Phi^{\text{loc}}_{UJ}[\mathbf{G}] + \Phi^{\text{cl}}_{\tilde{U}\tilde{J}}[\hat{P}_{t_{2g}}\mathbf{G}] - \Phi^{\text{loc}}_{\tilde{U}\tilde{J}}[\hat{P}_{t_{2g}}\mathbf{G}], \qquad (2)$$

where $\hat{P}_{t_{2g}}$ is the projector on t_{2g} orbitals. One can think of this as a selective improvement of the diagrammatic summation by going from single site to cluster DCA for the t_{2g} orbitals which is corrected by subtracting the double counting of the single site DMFT t_{2g} diagrams. The use of $\tilde{U}$ and $\tilde{J}$ reflects the screening of the bare interactions by the elimination of the e_g degrees of freedom in the cluster corrections. In the Appendix, we show how the screening is determined and how the mixed DMFT-DCA scheme is solved in practice. For the sake of completeness, the solution of the DMFT equations and the impurity models are detailed as well.

In the following, all energies are given in units of eV and the filling is constrained to 6 electrons per Fe atom. The upper panel in Fig. 2 shows the t_{2g} the self-energies obtained by DMFT and DCA at $T = 174K$, $(U,\tilde{U}) = (4.5, 4.5)$ and $(J,\tilde{J}) = (0.45, 0.375)$. The DCA self-energy is shown in a "real-space site basis" with local part $(\mathbf{\Sigma}_{\mathbf{K}=+} + \mathbf{\Sigma}_{\mathbf{K}=-})/2$ and non-local

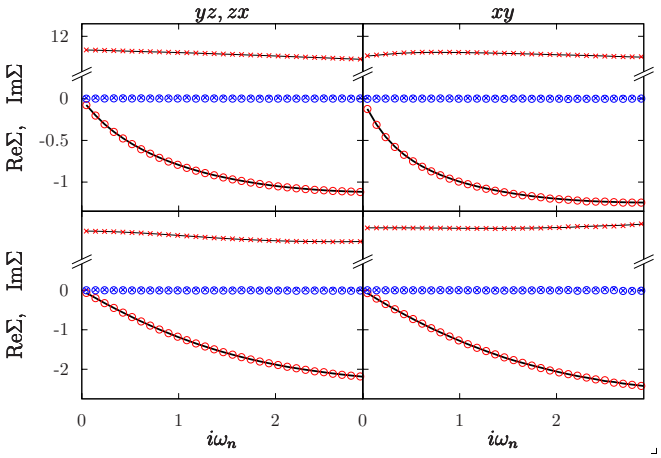

FIG. 2. (Color online) Comparison of the t_{2g} self-energy obtained by DMFT (real/imaginary part with thin/bold lines) and DCA (local/non-local part in red/blue and real/imaginary part with crosses/circles). All self-energies are diagonal in orbital space (see Appendix). The left panels show the degenerate yz, zx entries and the right panel shows the xy entry. The temperature is $T = 174K$. In the upper panels $(U,\tilde{U}) = (4.5, 4.5)$ and $(J,\tilde{J}) = (0.45, 0.375)$ while in the lower panels $(U,\tilde{U}) = (10.125, 9)$ and $(J,\tilde{J}) = (0, 0)$.

part $(\mathbf{\Sigma}_{\mathbf{K}=+} - \mathbf{\Sigma}_{\mathbf{K}=-})/2$. The non-local self-energy is essentially zero and the local self-energy is in excellent agreement with DMFT. The quasiparticle weight is $(Z_{yz/zx}, Z_{xy}) = (0.4, 0.3)$ and the filling of the t_{2g}-filling per Fe atom is $N_{t_{2g}} = 3.186$. To address the question wether this is due to the Hund's rule coupling or the orbital degeneracy, we set $J = 0$ but increase U in order to stay in a correlated regime, see lower panel in Fig. 2. The

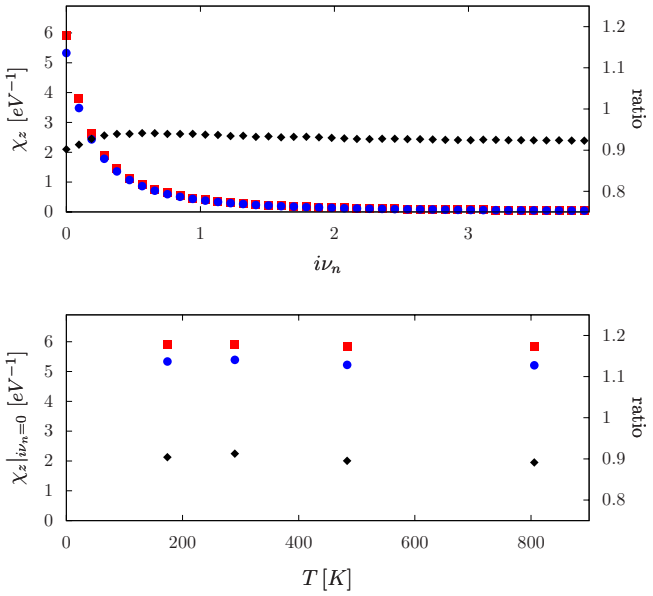

FIG. 3. (Color online) Impurity spin susceptibility (see Eq. 3) for DMFT (red squares) and DCA (blue circles) for parameters $(U, \tilde{U}) = (4.5, 4.5)$ and $(J, \tilde{J}) = (0.45, 0.375)$. The upper panel plots the susceptibility as a function of Matsubara frequencies for $T = 174K$. The lower panel plots the susceptibility as function of the temperature for $i\nu_n = 0$. The black diamonds display the ratio between the DMFT and DCA spin susceptibility, and its scale is displayed in the right y-axis.

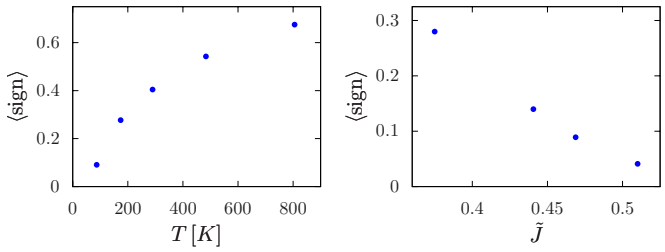

FIG. 4. Average sign in the CT-HYB simulations for the DCA impurity model, in the left panel for $(J, \tilde{J}) = (0.45, 0.375)$ as function of the temperature and in the right panel for $T = 174K$ as a function of the Hund's rule coupling (the values are $(J, \tilde{J}) = (0.45, 0.375)$, $(0.488, 0.441)$, $(0.506, 0.469)$ and $(0.525, 0.51)$ from left to right). The Coulomb repulsion is $(U, \tilde{U}) = (4.5, 4.5)$ in both panels. The CT-HYB simulations are carried out in the **K**-space single particle basis, see Appendix.

self-energies are local as well, $(Z_{yz/zx}, Z_{xy}) = (0.41, 0.39)$ and $N_{t_{2g}} = 2.77$.

Another question that arises is the locality at the two particle level. To this end, we measure the impurity spin susceptibility defined as

$$\chi_z(i\nu_n) = \frac{1}{N_{\mathcal{P}}} \int_0^\beta e^{i\nu_n \tau} \langle S_z^{t_{2g}}(\tau) S_z^{t_{2g}} \rangle d\tau, \qquad (3)$$

where $S_z^{t_{2g}}$ is the total spin along the z direction of the t_{2g} degrees of freedom on the impurity, for both DMFT ($N_{\mathcal{P}} = 1$) and DCA ($N_{\mathcal{P}} = 2$), see Fig. 3. We also plot the ratio of the DCA and DMFT susceptibility which is ≈ 0.9, meaning that even at the two particle level, our coarse graining does not show momentum space differentiation. This is very different from the cuprate case.

Fig. 4 shows the average sign in the CT-HYB simulations for the DCA impurity model for different temperatures and Hund's rule couplings. The sign rapidly drops with increasing Hund's rule coupling. This makes cluster simulations of materials with large mass renormalizations expensive, in particular at low temperatures.

To conclude, we have demonstrated that the local approximation describes well Hunds metals, such as many iron-pnictides and chalcogenides, in their normal state. In the region of large mass renormalizations, relevant to materials such as FeTe, there is an onset of a severe minus sign problem. In itself this does not prove non-locality of the self-energies, but the investigation of this region will require other impurity solvers and is outside the scope of this work. We have solved the same model Hamiltonian with other two site tiling of the Brillouin zone. The results support our conclusion that the self energy is local, with little tendency towards momentum space differentiation in the parameter range explored in this paper.

We can rationalize our results by noticing that orbital degeneracy generally makes the spin-spin correlations more classical and increases the frustration, making single site DMFT treatments more accurate, an effect noticed in early DMFT studies of orbitally degenerate systems[53]. However, other considerations may be important. Recently a three band Hamiltonian was studied at larger values of the interactions U and J and strong momentum space differentiation was found[54]. Notice however that they considered a different dispersion relation, suggesting that the dispersion of the iron pnictides is important.

Another possibility is that our cluster formulation is too small to produce sizable precursors of the magnetically ordered stripe state. Once these magnetic fluctuations are included, **k**-dependence in the self-energy will appear, as seen in the treatment of Ref. 55 with dual fermions. Notice however that these effects appear only sufficiently close to the magnetic transition, and our results will still remain valid at high temperatures where the correlation length is short.

We believe that our findings of locality do not depend of our treatment of the e_g orbitals, which is limited to single site DMFT. Treating them at the cluster DMFT level is less important as these orbitals contribute less to the Fermi surface. Confirming this by a full cluster DMFT calculation including all 5 orbitals remains an interesting open problem for the future.

We also comment on the role of non-local interactions. These interactions play two roles. First, they generate a **k**-dependence in the self-energy at the Hartree-Fock level, but this effect should be thought of as already included in the bare dispersions used as input to our studies. Sec-

ond, the frequency dependence of the self-energy due to non-local Coulomb interactions has been shown to be important in cluster DMFT studies of Ti_2O_3[56]. The study of this effect on pnictides and its possible relevance to the nematic transition was recently suggested in Ref. 57, which studied at the Hartree-Fock level. This work can be extended using the methods of this paper, and is left for future work.

More generally the methodology introduced in this paper to treat different degrees of freedom at different levels of approxmation should be widely applicable. This will be useful for treating systems with multiple degrees of freedom exhibiting different levels of non locality or different levels of correlation.

This work was supported by DOE DE-FG02-99ER45761 (P.S. and G.K.) and NSF-DMR1405303 (K.H.). This research used resources of the Oak Ridge Leadership Computing Facility at the Oak Ridge National Laboratory, which is supported by the Office of Science of the US Department of Energy under Contract No. DE-AC05-00OR22725.

APPENDIX

We begin here by writing down the equations for the the mixed DMFT-DCA scheme as defined by Eqs. 1 and 2 by means of impurity models. We then show how the effective interactions $\tilde{U}$ and $\tilde{J}$ are determined and the equations are solved in practice. Finally, we detail the impurity models.

A. Mixed DMFT-DCA equations

The functional derivative of Eq. 2 yields the approximation

$$\mathbf{\Sigma}(\mathbf{k}) = \begin{pmatrix} \mathbf{\Sigma}^{\rm loc}_{t_{2g}} + \tilde{\mathbf{\Sigma}}^{\rm cl}_{\mathbf{K}} - \tilde{\mathbf{\Sigma}}^{\rm loc} & 0 \\ 0 & \mathbf{\Sigma}^{\rm loc}_{e_g} \end{pmatrix} \tag{4}$$

for the lattice self-energy written in $\mathbf{k}$-space, where $\mathbf{K} = +$ ($\mathbf{K} = -$) if $\mathbf{k}$ lies in the patch $\mathcal{P}_+$ ($\mathcal{P}_-$). The self-energies on the right hand side of Eq. 4 are identified with those of impurity models as follows:

(a) $\mathbf{\Sigma}^{\rm loc}$, a diagonal 5×5 matrix in d-shell orbital space with components $\mathbf{\Sigma}^{\rm loc}_{t_{2g}}$ and $\mathbf{\Sigma}^{\rm loc}_{e_g}$, is the self-energy of a single site d-shell impurity model with interactions U and J.

(b) $\tilde{\mathbf{\Sigma}}^{\rm loc}$, a diagonal 3×3 matrix in t_{2g} orbital space, is the self-energy of a single site t_{2g}-orbital impurity model with effective interactions $\tilde{U}$ and $\tilde{J}$.

(c) $\tilde{\mathbf{\Sigma}}^{\rm cl}_{\mathbf{K}}$, a diagonal 3×3 matrix in t_{2g} orbital space for each $\mathbf{K}$, is the self-energy of a two-site t_{2g}-orbital cluster impurity model with effective interactions $\tilde{U}$ and $\tilde{J}$.

The non-interacting part of these impurity models is encapsulated in the Weiss-Fields $\mathbf{G}^{\rm loc}_0$, $\tilde{\mathbf{G}}^{\rm loc}_0$ and $\tilde{\mathbf{G}}^{\rm cl}_{0\mathbf{K}}$, which relate the self-energies with the interacting Greens functions $\mathbf{G}^{\rm loc}$, $\tilde{\mathbf{G}}^{\rm loc}$ and $\tilde{\mathbf{G}}^{\rm cl}_{\mathbf{K}}$ through the Dyson equations

$$(\mathbf{G}^{\rm loc})^{-1} = (\mathbf{G}^{\rm loc}_0)^{-1} - \mathbf{\Sigma}^{\rm loc} \tag{5a}$$
$$(\tilde{\mathbf{G}}^{\rm loc})^{-1} = (\tilde{\mathbf{G}}^{\rm loc}_0)^{-1} - \tilde{\mathbf{\Sigma}}^{\rm loc} \tag{5b}$$
$$(\tilde{\mathbf{G}}^{\rm cl}_{\mathbf{K}})^{-1} = (\tilde{\mathbf{G}}^{\rm cl}_{0\mathbf{K}})^{-1} - \tilde{\mathbf{\Sigma}}^{\rm cl}_{\mathbf{K}}. \tag{5c}$$

Eq. 4 yields the approximate lattice Green function

$$\mathbf{G}^{-1}(\mathbf{k}) = \mathbf{G}^{-1}_0(\mathbf{k}) - \mathbf{\Sigma}(\mathbf{k}), \tag{6}$$

where $\mathbf{G}^{-1}_0(i\omega_n, \mathbf{k}) = i\omega_n + \mu - \mathbf{h}_0(\mathbf{k})$ is the bare lattice Green function. The DMFT and DCA approximations of the Luttinger-Ward functional then require

$$\mathbf{G}^{\rm loc} = \frac{1}{|\mathrm{BZ}|}\int_{\mathrm{BZ}} d\mathbf{k}\mathbf{G}(\mathbf{k}) \tag{7a}$$
$$\tilde{\mathbf{G}}^{\rm loc} = \frac{1}{|\mathrm{BZ}|}\int_{\mathrm{BZ}} d\mathbf{k}\hat{P}_{t_{2g}}\mathbf{G}(\mathbf{k}) \tag{7b}$$
$$\tilde{\mathbf{G}}^{\rm cl}_{\mathbf{K}} = \frac{1}{|\mathcal{P}_{\mathbf{K}}|}\int_{\mathcal{P}_{\mathbf{K}}} d\mathbf{k}\hat{P}_{t_{2g}}\mathbf{G}(\mathbf{k}). \tag{7c}$$

Fixing the chemical potential by imposing 6 electrons per atom, above equations determine the Weiss-Fields and hereby the solution of the mixed DMFT-DCA scheme. The interactions U and J are taken as external parameters, and what remains to be determined are the effective interactions $\tilde{U}$ and $\tilde{J}$ which take into account the screening of the t_{2g} degrees of freedom in the cluster corrections.

Notice here that, in the normal phase, the DMFT self-energies $\mathbf{\Sigma}^{\rm loc}$ and $\tilde{\mathbf{\Sigma}}^{\rm loc}$ (and also $\mathbf{G}^{\rm loc}_0$, $\tilde{\mathbf{G}}^{\rm loc}_0$, $\mathbf{G}^{\rm loc}$ and $\tilde{\mathbf{G}}^{\rm loc}$) are diagonal in the orbital space. This comes from the D_{2d} point symmetry group of an Fe atom. Furthermore, the patches are invariant under this symmetry group, so that the DCA self-energy $\tilde{\mathbf{\Sigma}}^{\rm cl}_{\mathbf{K}}$ (and also $\tilde{\mathbf{G}}^{\rm cl}_{0\mathbf{K}}$ and $\tilde{\mathbf{G}}^{\rm cl}_{\mathbf{K}}$) is diagonal in the orbital space as well.

B. Effective interactions

To determine the effective interactions, we define an effective problem where correlations are applied only to the t_{2g} orbitals. These effective correlations, which are identified with $\tilde{U}$ and $\tilde{J}$, are then determined by requiring that this model reproduces at low energies the results of the five band calculation (with correlations U and J), *when both models are solved via single site DMFT*. We use the following algorithm:

(i) The five band model is solved with single site DMFT for a filling of 6 d-shell electrons per Fe atom and interactions U and J. This yields a local lattice self-energy $\mathbf{\Sigma}^{\rm loc}$ (with components $\mathbf{\Sigma}^{\rm loc}_{e_g}$ and $\mathbf{\Sigma}^{\rm loc}_{t_{2g}}$), a filling of the t_{2g} orbitals and a chemical potential.

(ii) We determine the low energy model by defining the effective bare lattice propagator

$$\tilde{\mathbf{G}}_0^{-1} := \mathbf{G}_0^{-1} - \begin{pmatrix} \Sigma^{\mathrm{HF}} \cdot \mathbf{1}_{t_{2g}} & 0 \\ 0 & \mathbf{\Sigma}^{\mathrm{loc}}_{e_g} \end{pmatrix}. \tag{8}$$

Here, $\mathbf{\Sigma}^{\mathrm{loc}}_{e_g}$ is the e_g part of the self-energy obtained in (i), and Σ^{HF} (which can be thought as an average Hartree-Fock contribution to the t_{2g} self-energy coming from the e_g orbitals) will be determined in the next step. The chemical potential is fixed to the value obtained in (i).

(iii) To determine Σ^{HF}, $\tilde{U}$ and $\tilde{J}$, we solve the problem with propagator Eq. 8 and the effective interactions applied to the t_{2g} orbitals with single-site DMFT. The resulting self-energy is denoted by $\tilde{\mathbf{\Sigma}}^{\mathrm{loc}}$. Σ^{HF} is determined by requiring that the t_{2g} filling is the same as in (i). Requiring that $\tilde{\mathbf{\Sigma}}^{\mathrm{loc}} + \Sigma^{\mathrm{HF}}$ matches $\mathbf{\Sigma}^{\mathrm{loc}}_{t_{2g}}$ at the lowest Matsubara frequencies determines the effective interactions $\tilde{U}$ and $\tilde{J}$.

It is remarkable that these requirements give us very good matching of the self-energies at all energies, as shown in Fig. 5.

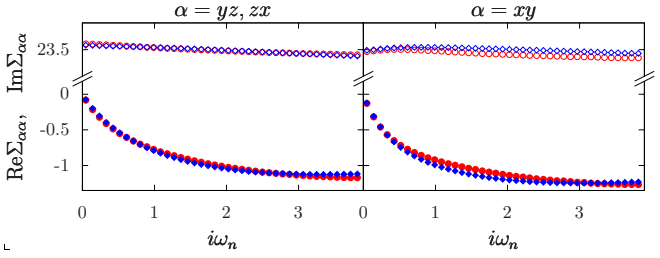

FIG. 5. (Color online) Self-energies (real/imaginary part with open/filled symbols) of the t_{2g} orbitals obtained with DMFT for the model with interactions applied to all d-shell orbitals (red circles) and for the effective t_{2g} model (blue diamonds). In the latter case, the Hartree-Fock constant Σ^{HF} is added. The parameters are $T = 174K$, $(U, \tilde{U}) = (4.5, 4.5)$ and $(J, \tilde{J}) = (0.45, 0.375)$.

C. Solving the mixed DMFT-DCA equations and the DMFT equation

The good agreement of the self-energies in Fig. 5 suggests to solve the mixed DMFT-DCA scheme in a simplified manner. Instead of simultaneously solving the three impurity models in Sec. A, we just apply DCA to the effective t_{2g} model used to determine the screened interactions $\tilde{U}$ and $\tilde{J}$. Σ^{HF} is slightly readjusted to preserve the t_{2g} filling found in Sec. B (i).

This simplified solution is justified *if the cluster corrections to local quantities is small*. Indeed, in this case we can start by ignoring the cluster corrections when solving the mixed DMFT-DCA scheme and solve the model with DMFT (which corresponds to step (i) in Sec. B). We then solve the model with cluster corrections (where $\tilde{U}$ and $\tilde{J}$ have been determined as discussed in Sec. B), keeping however the e_g self-energy $\mathbf{\Sigma}^{\mathrm{loc}}_{e_g}$ and the chemical potential obtained without cluster corrections fixed. Further, the contribution to the t_{2g} self-energy from $\mathbf{\Sigma}^{\mathrm{loc}}_{t_{2g}} - \tilde{\mathbf{\Sigma}}^{\mathrm{loc}}$ is replaced by a constant proportional to the identity, which is justified by Fig. 5. Choosing this constant Σ^{HF} to preserve the t_{2g} filling found in Sec. B (i), this amounts just to solve the effective t_{2g} model with DCA as mentioned above. Compared to the exact solution of the DMFT-DCA scheme, this simplified solution avoids stability issues and guaranties causality (c.f. nested cluster schemes in Ref. 58).

When comparing results from the mixed DMFT-DCA scheme with DMFT results, the latter is applied to the effective t_{2g} problem for the sake of coherence. The DMFT self-energy is thus $\tilde{\mathbf{\Sigma}}^{\mathrm{loc}}$ from Sec. B (iii), while the mixed DMFT-DCA self-energy is $\mathbf{\Sigma}^{\mathrm{cl}}_{\mathbf{K}}$, obtained in the above approximation.

D. Impurity Models

The aim here is to write down the action for the impurity models in Sec. A. To this end, we begin by detailing the interaction used in this work.

With respect to the d-shell single particle basis $|\sigma m\rangle$, where σ is the spin and the angular part is encapsulated in the spherical harmonics $Y^m_{l=2}$, the local interaction

$$\hat{V} = \frac{1}{2} \sum_{\sigma\sigma'} \sum_{\{m_i\}} V_{m_1 m_2 m_3 m_4} c^\dagger_{\sigma m_1} c^\dagger_{\sigma' m_2} c_{\sigma' m_3} c_{\sigma m_4} \tag{9}$$

is given by the tensor

$$\begin{aligned} V_{m_1 m_2 m_3 m_4} = & \sum_{k=0,2,4} \frac{4\pi}{2k+1} F^k \\ & \times \sum_{m=-k}^{k} \langle Y_2^{m_1} | Y_k^{m*} | Y_2^{m_4} \rangle \langle Y_2^{m_2} | Y_k^{m} | Y_2^{m_3} \rangle. \end{aligned} \tag{10}$$

The Slater-Condon parameters F^0, F^2 and F^4 encapsulate both the radial part of the single particle basis (which is the same for all $|\sigma m\rangle$) and the interaction. In this work we use $F^0 = U$, $F^2 = 14 \cdot J/1.625$ and $F^4 = 0.625 \cdot F^2$, where U is the Coulomb repulsion and J the Hund's rule coupling.

In solids, it is more convenient to work in the basis of real spherical harmonics $|\sigma\alpha\rangle$ with $\alpha \in \{yz, zx, xy, 3z^2 - r^2, x^2 - y^2\}$, and we denote the corresponding creation operators by $d^\dagger_{\sigma\alpha}$. We slightly simplify the interaction tensor $V_{\alpha_1\alpha_2\alpha_3\alpha_4}$ in this basis by setting all elements which are not of the form $V_{\alpha\alpha\alpha'\alpha'}$,$V_{\alpha\alpha'\alpha'\alpha}$ or $V_{\alpha\alpha'\alpha\alpha'}$ to zero. While this truncation preserves the spin $SU(2)$ invariance of the interaction Eqs. 9 and 10, the orbital $SO(3)$ invariance is lifted. However, the truncated interaction

is still D_{2d} invariant and the crystal fields in the present case lift the $SO(3)$ degeneracy anyway.

In the basis of real spherical harmonics, the action for the single-site d-shell impurity model Sec. A (a) reads

$$\begin{aligned} S = &- \sum_{\sigma} \sum_{\alpha} \iint_0^\beta d^\dagger_{\sigma\alpha}(\tau) G^{-1}_{0\alpha\alpha}(\tau - \tau') d_{\sigma\alpha}(\tau') d\tau d\tau' \\ &+ \frac{1}{2} \sum_{\sigma\sigma'} \sum_{\{\alpha_i\}} V^{UJ}_{\alpha_1\alpha_2\alpha_3\alpha_4} \int_0^\beta d^\dagger_{\sigma\alpha_1}(\tau) d^\dagger_{\sigma'\alpha_2}(\tau) \\ &\times d_{\sigma'\alpha_3}(\tau) d_{\sigma\alpha_4}(\tau) d\tau, \end{aligned} \tag{11}$$

where the superscript of the interaction tensor indicates that U and J enter the Slater-Condon parameters. Restricting in the action Eq. 11 the orbital sums to t_{2g} orbitals and replacing U, J and $\mathbf{G}_0$ by the effective $\tilde{U}$, $\tilde{J}$ and $\tilde{\mathbf{G}}_0$ respectively yields the single-site t_{2g} impurity model Sec. A (b).

The non-interacting part of the cluster impurity model action Sec. A (c) reads

$$\begin{aligned} S_0 = &- \sum_{\sigma} \sum_{\mathbf{K}=\pm} \sum_{\alpha \in t_{2g}} \iint_0^\beta d^\dagger_{\sigma\alpha\mathbf{K}}(\tau) \tilde{G}^{-1}_{0\mathbf{K}\alpha\alpha}(\tau - \tau') \\ &\times d_{\sigma\alpha\mathbf{K}}(\tau') d\tau d\tau', \end{aligned} \tag{12}$$

where $d^\dagger_{\sigma\alpha\mathbf{K}}$ creates an electron with spin σ and coarse grained momentum $\mathbf{K}$ in the orbital α. The interacting part, written in a "real-space site basis" $d_{\alpha\sigma 1} := (d_{\sigma\alpha+} + d_{\sigma\alpha-})/\sqrt{2}$ and $d_{\alpha\sigma 2} := (d_{\sigma\alpha+} - d_{\sigma\alpha-})/\sqrt{2}$, reads

$$\begin{aligned} S_I = &\frac{1}{2} \sum_{\sigma\sigma'} \sum_{a=1,2} \sum_{\{\alpha_i\} \in t_{2g}} V^{\tilde{U}\tilde{J}}_{\alpha_1\alpha_2\alpha_3\alpha_4} \\ &\times \int_0^\beta d^\dagger_{\sigma\alpha_1 a}(\tau) d^\dagger_{\sigma'\alpha_2 a}(\tau) d_{\sigma'\alpha_3 a}(\tau) d_{\sigma\alpha_4 a}(\tau) d\tau. \end{aligned} \tag{13}$$

For the CT-HYB simulations, the $\mathbf{K}$-space single particle basis $d^\dagger_{\sigma\mathbf{K}\alpha}$ is used.

[1] Y. Kamihara, H. Hiramatsu, M. Hirano, R. Kawamura, H. Yanagi, T. Kamiya, and H. Hosono, Journal of the American Chemical Society **128**, 10012 (2006).
[2] A. V. Chubukov and P. J. Hirschfeld, ArXiv e-prints (2014), arXiv:1412.7104 [cond-mat.supr-con].
[3] K. Haule and G. Kotliar, New Journal of Physics **11**, 025021 (2009).
[4] Z. P. Yin, K. Haule, and G. Kotliar, Nature Physics **advance online publication** (2011), 10.1038/nphys1923.
[5] J. Mravlje, M. Aichhorn, T. Miyake, K. Haule, G. Kotliar, and A. Georges, Phys. Rev. Lett. **106**, 096401 (2011).
[6] A. Georges, L. d. Medici, and J. Mravlje, Annual Review of Condensed Matter Physics **4**, 137 (2013).
[7] A. Georges, G. Kotliar, W. Krauth, and M. J. Rozenberg, Rev. Mod. Phys. **68**, 13 (1996).
[8] G. Kotliar, S. Y. Savrasov, G. Pálsson, and G. Biroli, Phys. Rev. Lett. **87**, 186401 (2001).
[9] T. Maier, M. Jarrell, T. Pruschke, and M. H. Hettler, Rev. Mod. Phys. **77**, 1027 (2005).
[10] X. Deng, A. Sternbach, K. Haule, D. N. Basov, and G. Kotliar, Phys. Rev. Lett. **113**, 246404 (2014).
[11] C. Huscroft, M. Jarrell, T. Maier, S. Moukouri, and A. N. Tahvildarzadeh, Phys. Rev. Lett. **86**, 139 (2001).
[12] A. I. Lichtenstein and M. I. Katsnelson, Phys. Rev. B **62**, R9283 (2000).
[13] M. Jarrell, T. Maier, M. H. Hettler, and A. N. Tahvildarzadeh, EPL (Europhysics Letters) **56**, 563 (2001).
[14] M. Jarrell, T. Maier, C. Huscroft, and S. Moukouri, Phys. Rev. B **64**, 195130 (2001).
[15] K. Haule, A. Rosch, J. Kroha, and P. Wölfle, Phys. Rev. B **68**, 155119 (2003).
[16] O. Parcollet, G. Biroli, and G. Kotliar, Phys. Rev. Lett. **92**, 226402 (2004).
[17] E. C. Carter and A. J. Schofield, Phys. Rev. B **70**, 045107 (2004).
[18] M. Civelli, M. Capone, S. S. Kancharla, O. Parcollet, and G. Kotliar, Phys. Rev. Lett. **95**, 106402 (2005).
[19] T. D. Stanescu and G. Kotliar, Phys. Rev. B **74**, 125110 (2006).
[20] B. Kyung, S. S. Kancharla, D. Sénéchal, A.-M. S. Tremblay, M. Civelli, and G. Kotliar, Phys. Rev. B **73**, 165114 (2006).
[21] A. Macridin, M. Jarrell, T. Maier, P. R. C. Kent, and E. D'Azevedo, Phys. Rev. Lett. **97**, 036401 (2006).
[22] K. Haule and G. Kotliar, Phys. Rev. B **76**, 092503 (2007).
[23] Y. Z. Zhang and M. Imada, Phys. Rev. B **76**, 045108 (2007).
[24] M. Civelli, M. Capone, A. Georges, K. Haule, O. Parcollet, T. D. Stanescu, and G. Kotliar, Phys. Rev. Lett. **100**, 046402 (2008).
[25] M. Civelli, Phys. Rev. B **79**, 195113 (2009).
[26] A. Liebsch and N.-H. Tong, Phys. Rev. B **80**, 165126 (2009).
[27] S. Sakai, Y. Motome, and M. Imada, Phys. Rev. Lett. **102**, 056404 (2009).
[28] P. Werner, E. Gull, O. Parcollet, and A. J. Millis, Phys. Rev. B **80**, 045120 (2009).
[29] E. Gull, M. Ferrero, O. Parcollet, A. Georges, and A. J. Millis, Phys. Rev. B **82**, 155101 (2010).
[30] N. Lin, E. Gull, and A. J. Millis, Phys. Rev. B **82**, 045104 (2010).
[31] G. Sordi, P. Sémon, K. Haule, and A.-M. S. Tremblay, Sci. Rep. **2** (2012), 10.1038/srep00547.
[32] G. Sordi, P. Sémon, K. Haule, and A.-M. S. Tremblay, Phys. Rev. B **87**, 041101 (2013).
[33] E. Gull, O. Parcollet, and A. J. Millis, Phys. Rev. Lett. **110**, 216405 (2013).
[34] E. Gull and A. J. Millis, Phys. Rev. B **88**, 075127 (2013).
[35] M. Imada, S. Sakai, Y. Yamaji, and Y. Motome, Journal of Physics: Conference Series **449**, 012005 (2013).
[36] G. Biroli and G. Kotliar, Phys. Rev. B **65**, 155112 (2002).
[37] K. Aryanpour, T. A. Maier, and M. Jarrell, Phys. Rev. B **71**, 037101 (2005).
[38] G. Biroli and G. Kotliar, Phys. Rev. B **71**, 037102 (2005).

[39] T. A. Maier, M. Jarrell, T. C. Schulthess, P. R. C. Kent, and J. B. White, Phys. Rev. Lett. **95**, 237001 (2005).
[40] B. Kyung, G. Kotliar, and A.-M. S. Tremblay, Phys. Rev. B **73**, 205106 (2006).
[41] S. Sakai, G. Sangiovanni, M. Civelli, Y. Motome, K. Held, and M. Imada, Phys. Rev. B **85**, 035102 (2012).
[42] Z. P. Yin, K. Haule, and G. Kotliar, Nat Phys **10**, 845 (2014).
[43] D. Guterding, S. Backes, H. O. Jeschke, and R. Valentí, Phys. Rev. B **91**, 140503 (2015).
[44] M. Aichhorn, S. Biermann, T. Miyake, A. Georges, and M. Imada, Phys. Rev. B **82**, 064504 (2010).
[45] J. M. Tomczak, M. van Schilfgaarde, and G. Kotliar, Phys. Rev. Lett. **109**, 237010 (2012).
[46] M. Ferrero, P. S. Cornaglia, L. De Leo, O. Parcollet, G. Kotliar, and A. Georges, Phys. Rev. B **80**, 064501 (2009).
[47] M. J. Calderón, B. Valenzuela, and E. Bascones, Phys. Rev. B **80**, 094531 (2009).
[48] This corresponds to choose $(pd\sigma)^2/|\epsilon_d - \epsilon_p| = 0.75eV$ in Ref.[47].
[49] E. Gull, A. J. Millis, A. I. Lichtenstein, A. N. Rubtsov, M. Troyer, and P. Werner, Rev. Mod. Phys. **83**, 349 (2011).
[50] K. Haule, Phys. Rev. B **75**, 155113 (2007).
[51] P. Sémon, C.-H. Yee, K. Haule, and A.-M. S. Tremblay, Phys. Rev. B **90**, 075149 (2014).
[52] J. M. Luttinger and J. C. Ward, Phys. Rev. **118**, 1417 (1960).
[53] H. Kajueter and G. Kotliar, International Journal of Modern Physics B **11**, 729 (1997).
[54] Y. Nomura, S. Sakai, and R. Arita, Phys. Rev. B **91**, 235107 (2015).
[55] A. N. Rubtsov, M. I. Katsnelson, and A. I. Lichtenstein, Phys. Rev. B **77**, 033101 (2008).
[56] A. I. Poteryaev, A. I. Lichtenstein, and G. Kotliar, Phys. Rev. Lett. **93**, 086401 (2004).
[57] K. Jiang, J. Hu, H. Ding, and Z. Wang, Phys. Rev. B **93**, 115138 (2016).
[58] G. Biroli, O. Parcollet, and G. Kotliar, Phys. Rev. B **69**, 205108 (2004).